A Paper-Based Microfluidic Fuel Cell with Hydrogen Peroxide as Fuel and Oxidant

Xiaohui Yan,[a] Ao Xu,[a] Lin Zeng,[a] Ping Gao,[b] and Tianshou Zhao*[a]

The ever-growing interest in portable electronics, especially wearable devices, imposes great demands on power sources that are compact. A paper-based microfluidic fuel cell for portable electronics that uses H_2O_2 as both fuel and oxidant is reported herein. Unlike conventional microfluidic fuel cells, which rely on a colaminar flow of anolyte and catholyte, the present fuel cell is realized by the selective catalysis of H_2O_2, and it can eliminate concerns about fuel management and disturbance by bubbles. Silver nanowires and carbon nanotube (CNT)-supported Prussian Blue are chosen as the anode and cathode catalyst, respectively, to catalyze the oxidation and reduction reactions. Results show that the present microfluidic fuel cell system is able to offer a peak power density as high as $0.88\,mW\,cm^{-2}$. Additional striking features of the present fuel cell are that it does not require precious-metal catalysts and the used fuel, H_2O_2, is a carbon-free and sustainable energy carrier.

Fuel cells have been widely regarded as the next generation of power sources due to their unique advantages of high efficiency and zero emission of pollutants.[1–3] For example, the proton exchange membrane fuel cell (PEMFC) is suitable for transportation applications due to its high power density and low operating temperature;[4–7] the solid oxide fuel cell (SOFC) has been developed for stationary power generation because its efficiency can be much higher than that of a thermal power station for converting fuel into electricity.[7–10] Recently, the usage of portable electronics, especially wearable devices, has attracted great attention in various fields, including medicine, fitness, and entertainment. However, the ever-growing range of wearable devices imposes great demands on operation time that current lithium-ion batteries or fuel cells are unable to meet. Therefore, new power sources are needed for such devices, and a power source as compact as possible is preferred. To meet this requirement, a novel fuel cell system, named the microfluidic fuel cell, has been developed.[11]

A microfluidic fuel cell is a system that integrates the delivery of reactants and removal of products.[12–14] The electrochemical reaction sites and electrode structure of this fuel cell are all realized on a microfluidic channel. The operating conditions for this system are based on a colaminar flow of fuel and oxidant, which forms a liquid–liquid interface to separate the anode and cathode; thus the use of a membrane can be eliminated in the microfluidic fuel cell. Efforts have been devoted to design workable microfluidic fuel cell systems.[15–17] For instance, a formic acid microfluidic fuel cell was proposed by Choban et al., in which formic acid was as the fuel and oxygen dissolved in a solution of sulfuric acid acted as the oxidant.[18] Sun et al. developed a formic acid–potassium permanganate colaminar flow fuel cell, which could output a maximum power of about $0.6\,mW\,cm^{-2}$.[19] In addition, H_2 (aq; sat)–O_2 (aq; sat),[20] methanol–O_2 (aq; sat),[21] ethanol–O_2 (aq; sat),[22] and glucose–O_2 (aq; sat) microfluidic fuel cells[23] have also been proposed.

Although promising, such colaminar microfluidic fuel cells encounter several limitations. First, fuel cell operation relies on the colaminar flow to form a stable liquid–liquid interface, which requires the Reynolds (Re) number to be small to avoid the occurrence of turbulence. This means that the size of the fuel cell cannot be scaled up, which makes it suitable for use in miniature devices only. Second, during the fuel cell discharging process, gaseous products will be generated and a two-phase flow will form, which makes the flow characteristics difficult to control and predict.[24] Third, a conventional microfluidic fuel cell requires two different aqueous solutions of anolyte and catholyte to power the wearable devices, so the system complexity significantly increases.

Herein, we propose a one-component, one-reactant microfluidic fuel cell to address the abovementioned issues. This type of fuel cell is fabricated from filter paper and uses H_2O_2 as both fuel and oxidant to eliminate the need for a colaminar flow (as shown in Figure 1). The dual role of H_2O_2 is realized by selective catalysis, which adopts silver nanowires (NWs) to catalyze the oxidation reaction and carbon nanotube (CNT)-supported Prussian Blue (PB) to catalyze the reduction reaction. In addition, this fuel cell system has the following striking features: 1) the fuel used, H_2O_2, is a carbon-free and sustainable energy carrier;[25] and 2) no precious-metal catalysts are required. Thus, the combined features of the microfluidic fuel cell and H_2O_2 contribute to potentially widespread applications in portable devices.

Figure 1 illustrates the working principle of the proposed fuel cell system. In this system, hydrogen peroxide acts as both fuel and oxidant, as realized by the selective catalysis of H_2O_2 with two different catalysts. At the anode [Eq. (1); SHE = standard hydrogen electrode], the hydrogen peroxide

[a] Dr. X. Yan, A. Xu, Dr. L. Zeng, Prof. T. S. Zhao
Department of Mechanical Engineering
The Hong Kong University of Science and Technology
Clear Water Bay, Kowloon, Hong Kong (SAR China)
E-mail: metzhao@ust.hk

[b] Prof. P. Gao
Department of Chemical and Biomolecular Engineering
The Hong Kong University of Science and Technology
Clear Water Bay, Kowloon, Hong Kong (SAR China)

(iD) The ORCID identification number(s) for the author(s) of this article can be found under https://doi.org/10.1002/ente.201700470.
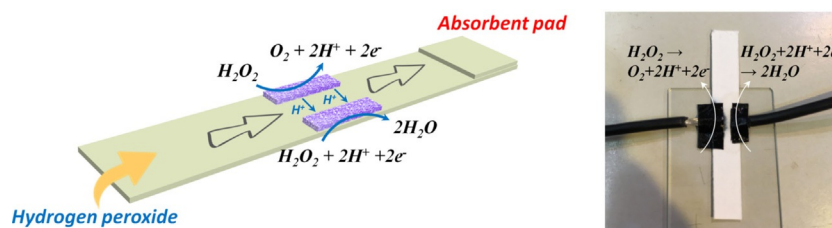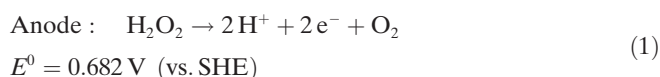
Figure 1. Schematic illustration of a paper-based hydrogen peroxide–hydrogen peroxide fuel cell (left), and a photograph of the fabricated demo (right).

oxidation reaction (HPOR) occurs, which generates protons, electrons, and oxygen.[26]

$$\text{Anode}: \quad H_2O_2 \rightarrow 2H^+ + 2e^- + O_2$$
$$E^0 = 0.682\,V \ (\text{vs. SHE}) \tag{1}$$

Electrons that are released pass through the external circuit to power the electronic device and then reach the cathode. Protons migrate from the anode to the cathode through electrolyte-saturated paper. At the cathode [Eq. (2)], the hydrogen peroxide reduction reaction (HPRR) takes place with electrons from the external circuit, protons through the "membrane", and oxygen from ambient air.

$$\text{Cathode}: \quad H_2O_2 \rightarrow 2H^+ + 2e^- \rightarrow 2H_2O$$
$$E^0 = 1.77\,V \ (\text{vs. SHE}) \tag{2}$$
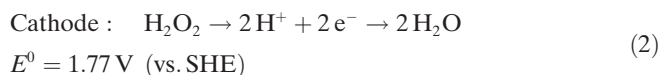
The overall reaction is given by Equation (3):

$$2H_2O_2 \rightarrow 2H_2O + O_2$$
$$E^0 = 1.09\,V \ (\text{vs. SHE}) \tag{3}$$

Theoretically, the open-circuit voltage (OCV) is as high as 1.09 V, which is comparable with that of a conventional hydrogen–oxygen fuel cell (1.23 V).

The key to realize the proposed fuel cell system is the selective catalysis of H_2O_2 because H_2O_2 can act as both an electron donor and an electron acceptor. Silver is chosen as the anode catalyst because the HPOR is preferred over the silver surface.[27] Silver NWs are used, rather than other types of nanostructure, to utilize the 1D geometry to enhance electron transfer for improved catalytic activity. A TEM image of an Ag NW is given in Figure 2a, which shows that the diameter of the NW is 120 nm. PB is chosen as an effective electrocatalyst towards the HPRR, as proven in our previous work.[28] Because PB itself is insulating, CNTs are used as the supporting material to form continuous pathways for electron transfer. A TEM image of the prepared PB/CNT is shown in Figure 2b, which clearly reveals the morphology of the CNT and PB nanoparticles. The PB nanoparticles, with sizes of tens of nanometers, are uniformly distributed onto CNT, which assures high conductivity.

Figure 3 shows the OCV values of the proposed fuel cell system. In the initial stages, the OCV gradually decreases over time due to the unsteady flow of electrolyte within the
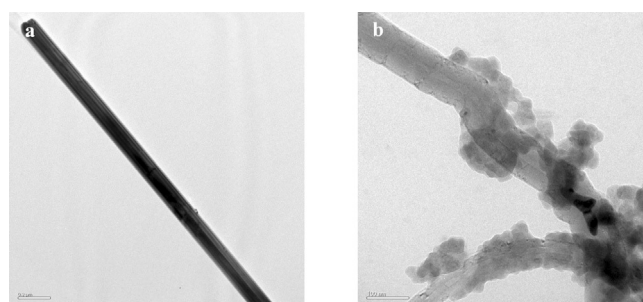

Figure 2. TEM images of a) the anode catalyst Ag NW; scale bar 0.2 μm; and b) the cathode catalyst, CNT-supported PB; scale bar 100 nm.
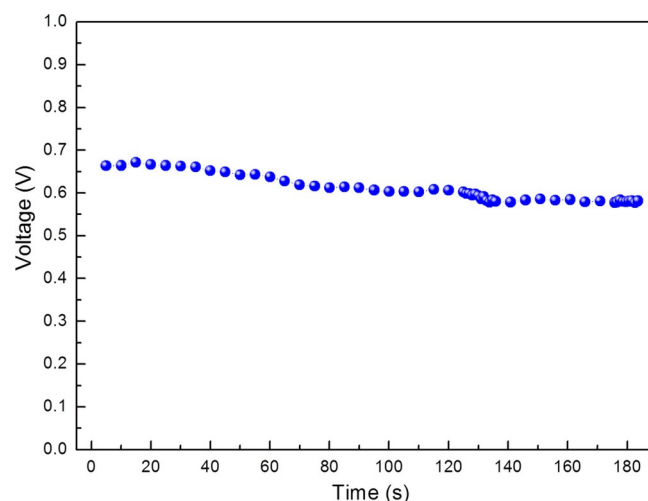

Figure 3. The OCV values in measurements of the H_2O_2 microfluidic fuel cell performance.

paper strip. After 140 s, the OCV stabilizes at 0.58 V, when a steady flow is achieved, which demonstrates that a continuous flow can be maintained by capillary action without the assistance of an external pump. The discrepancy between the theoretical OCV (1.09 V) and practical OCV (0.58 V) is due to the HPOR, which occurs at the cathode and is driven by the high potential. Simultaneous reduction and oxidation reactions taking place on one electrode would result in a mixed potential, which would significantly lower the practical voltage of the fuel cell. In addition, because oxygen is produced in the fuel cell, as indicated in Equation (1), the oxygen reduction reaction could also occur at the cathode [Eq. (4)]:

$$O_2 + 4\,H^+ + 4\,e^- \rightarrow 2\,H_2O$$
$$E^0 = 1.23\,V \ (vs.\,SHE) \tag{4}$$

which would further intensify the mixed-potential issue.

The cell performance is recorded at room temperature by using $2.0\,M$ H_2O_2 in a $1.5\,M$ solution of H_2SO_4 as the fuel and oxidant. Figure 4a shows the polarization and power density curves of the proposed microfluidic fuel cell. The peak density reaches as high as $0.88\,mW\,cm^{-2}$ for this microfluidic fuel cell.

The ohmic resistance was measured to be about $84.6\,\Omega$, which was much higher than that of a conventional proton exchange membrane because the distance between two catalyst layers (CLs) was several millimeters, greatly enlarging the proton transport distance compared with that of a conventional fuel cell, the membrane thickness of which was tens of micrometers only. The *IR*-free polarization curve is also given in Figure 4a, which still indicates a large overpotential after *IR* correction. Therefore, it can be concluded that the main loss in polarization comes from a loss in activation, which is derived from relatively sluggish electrochemical reactions of hydrogen peroxide. The discharging behavior
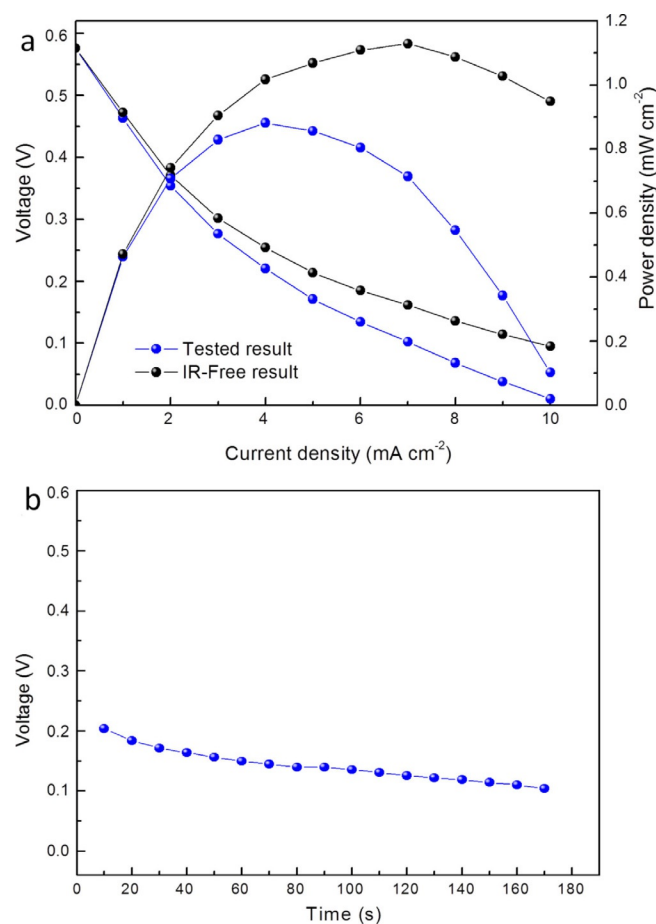
at $4\,mA\,cm^{-2}$ is shown in Figure 4b, for which a relatively stable performance is observed.

In summary, Figure 5 depicts a schematic illustration of a sustainable energy cycle based on H_2O_2. Hydrogen peroxide has been demonstrated as a promising solar fuel with a high energy density,[29] which can be produced from water and oxygen through photocatalytic reactions. Meanwhile, H_2O_2 can be used as a fuel and oxidant in our proposed fuel cell system to generate electricity to power portable devices with products of water and oxygen only. By combining these two procedures, a CO_2-free, eco-friendly, and sustainable energy cycle can be built.
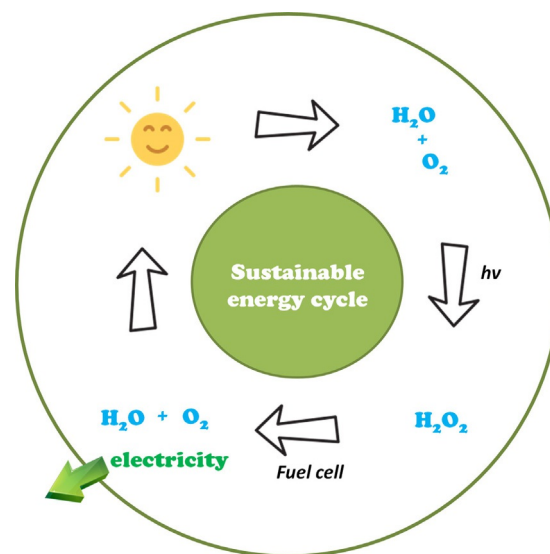
Figure 5. Schematic illustration of sustainable energy cycles based on H_2O_2.

Figure 4. a) Polarization curve of the H_2O_2 microfluidic fuel cell recorded at room temperature with $2.0\,M$ H_2O_2 in a $1.5\,M$ solution of H_2SO_4. b) Constant-current discharging behavior at a current density of $4\,mA\,cm^{-2}$.

Experimental Section

Catalysts

Commercially available Ag NWs purchased from Nanjing XFNANO Materials Tech Co., Ltd, were used as the anode catalyst and homemade CNT-supported PB was chosen as the cathode catalyst. The synthesis of PB/CNT was reported elsewhere.[28,30] In brief, CNTs were suspended in a $0.1\,M$ solution of HCl and stirred in an ultrasonic water bath to form a slurry. Next, the required amount of $0.5\,M$ $K_3[Fe(CN)_6]$ in a $0.1\,M$ solution of HCl was added to the slurry dropwise, followed by $0.5\,M$ $FeCl_3$ in $0.1\,M$ HCl. The mass ratio of CNT to PB was controlled to be 1:2 to ensure high electric conductivity. The resulting mixture was stirred for 1 h and the entire process was maintained at room temperature. The resulting slurry (PB/CNT) was collected by filtration and thoroughly washed with $0.1\,M$ HCl until the washing solution became colorless. The product was then dried at $100\,°C$ for 3 h and then stored in the dark in a desiccator.

Catalyst layer

The anode catalyst ink was prepared by dispersing Ag NWs into ethanol with a solution of Nafion (5 wt %, Dupont), followed by ultrasonic treatment to form the homogeneous slurry. The catalyst ink was then directly painted onto the paper strip to form

the anode CL, in which the Ag loading was $2.0\,\mathrm{mg\,cm^{-2}}$ and the mass ratio of Nafion ionomer was $20\,\mathrm{wt\%}$. The same procedure was used to prepare the cathode CL, in which the PB/CNT loading and Nafion content were also $2.0\,\mathrm{mg\,cm^{-2}}$ and $20\,\mathrm{wt\%}$, respectively. The active size of each CL was $0.5\,\mathrm{cm} \times 0.2\,\mathrm{cm}$.

Fuel cell system

A paper strip, made from filter paper (Whatman), with a size of $1\,\mathrm{cm} \times 8\,\mathrm{cm}$, composed the integral structure of the one-component microfluidic fuel cell. The CL was located in the middle of the paper strip, as shown in Figure 1. Two pieces of carbon paper (Toray 060) were connected with CLs to function as the current collector. The inlet of the paper strip was connected with a chamber filled with $2.0\,\mathrm{M}\ H_2O_2$ in a $1.5\,\mathrm{M}$ solution of H_2SO_4, which worked as both fuel and oxidant. The other end of the paper strip was covered by an absorbent pad consisting of additional several layers of the same filter papers. Thus, continuous flow could be maintained by capillary action within the paper during fuel cell operation, which eliminated the need for external pumps.

Acknowledgement

Conflict of interest

The authors declare no conflict of interest.

[1] S. K. Kamarudin, F. Achmad, W. R. W. Daud, *Int. J. Hydrogen Energy* **2009**, *34*, 6902–6916.
[2] V. Mehta, J. S. Cooper, *J. Power Sources* **2003**, *114*, 32–53.
[3] H. Liu, C. Song, L. Zhang, J. Zhang, H. Wang, D. P. Wilkinson, *J. Power Sources* **2006**, *155*, 95–110.
[4] S. J. Peighambardoust, S. Rowshanzamir, M. Amjadi, *Int. J. Hydrogen Energy* **2010**, *35*, 9349–9384.
[5] W. Dai, H. Wang, X. Z. Yuan, J. J. Martin, D. Yang, J. Qiao, J. Ma, *Int. J. Hydrogen Energy* **2009**, *34*, 9461–9478.
[6] X. H. Yan, T. S. Zhao, L. An, G. Zhao, L. Zeng, *Appl. Energy* **2015**, *138*, 331–336.
[7] X. H. Yan, R. Wu, J. B. Xu, Z. Luo, T. S. Zhao, *J. Power Sources* **2016**, *311*, 188–194.
[8] N. Shaigan, W. Qu, D. G. Ivey, W. Chen, *J. Power Sources* **2010**, *195*, 1529–1542.
[9] S. C. Singhal, *Solid State Ionics* **2000**, *135*, 305–313.
[10] C. Sun, U. Stimming, *J. Power Sources* **2007**, *171*, 247–260.
[11] E. Kjeang, N. Djilali, D. Sinton, *J. Power Sources* **2009**, *186*, 353–369.
[12] K. H. Purohit, S. Emrani, S. Rodriguez, S. S. Liaw, L. Pham, V. Galvan, K. Domalaon, F. A. Gomez, J. L. Haan, *J. Power Sources* **2016**, *318*, 163–169.
[13] V. Galvan, K. Domalaon, C. Tang, S. Sotez, A. Mendez, M. J. Heravi, K. Purohit, L. Pham, J. Haan, F. A. Gomez, *Electrophoresis* **2016**, *37*, 504–510.
[14] T. S. Copenhaver, K. H. Purohit, K. Domalaon, L. Pham, B. J. Burgess, N. Manorothkul, V. Galvan, S. Sotez, F. A. Gomez, J. L. Haan, *Electrophoresis* **2015**, *36*, 1825–1829.
[15] D. Sinton, *Lab Chip* **2014**, *14*, 3127–3134.
[16] M. A. Modestino, D. Fernandez Rivas, S. M. H. Hashemi, J. G. E. Gardeniers, D. Psaltis, *Energy Environ. Sci.* **2016**, *9*, 3381–3391.
[17] S. M. H. Hashemi, M. Neuenschwander, P. Hadikhani, M. A. Modestino, D. Psaltis, *J. Power Sources* **2017**, *348*, 212–218.
[18] E. R. Choban, L. J. Markoski, A. Wieckowski, P. J. A. Kenis, *J. Power Sources* **2004**, *128*, 54–60.
[19] M. H. Sun, G. V. Casquillas, S. S. Guo, J. Shi, H. Ji, Q. Ouyang, Y. Chen, *Microelectron. Eng.* **2007**, *84*, 1182–1185.
[20] J. L. Cohen, D. J. Volpe, D. A. Westly, A. Pechenik, H. D. Abruna, *Langmuir* **2005**, *21*, 3544–3550.
[21] J. P. Esquivel, F. J. D. Campo, F. J. L. Gomez, S. Rojas, N. Sabate, *Energy Environ. Sci.* **2014**, *7*, 1744–1749.
[22] A. J. Armenta-González, R. Carrera-Cerritos, A. Moreno-Zuria, L. Álvarez-Contreras, J. Ledesma-García, F. M. Cuevas-Muñiz, L. G. Arriaga, *Fuel* **2016**, *167*, 240–247.
[23] M. Togo, A. Takamura, T. Asai, H. Kaji, M. Nishizawa, *J. Power Sources* **2008**, *178*, 53–58.
[24] J. C. Shyu, C. S. Wei, C. J. Lee, C. C. Wang, *Appl. Therm. Eng.* **2010**, *30*, 1863–1871.
[25] L. An, T. Zhao, X. Yan, X. Zhou, P. Tan, *Sci. Bull.* **2015**, *60*, 55–64.
[26] A. E. Sanli, *Int. J. Energy Res.* **2013**, *37*, 1488–1497.
[27] D. He, S. Garg, T. D. Waite, *Langmuir* **2012**, *28*, 10266–10275.
[28] X. H. Yan, T. S. Zhao, L. An, G. Zhao, L. Shi, *Int. J. Hydrogen Energy* **2016**, *41*, 5135–5140.
[29] S. Kato, J. Jung, T. Suenobu, S. Fukuzumi, *Energy Environ. Sci.* **2013**, *6*, 3756–3764.
[30] F. Ricci, A. Amine, C. S. Tuta, A. A. Ciucu, F. Lucarelli, G. Palleschi, D. Moscone, *Anal. Chim. Acta* **2003**, *485*, 111–120.